sustainability

MDPI

Article

A High-Efficiency Voltage Equalization Scheme for Supercapacitor Energy Storage System in Renewable Generation Applications

Liran Li, Zhiwu Huang *, Heng Li and Honghai Lu

School of Information Science and Engineering, Central South University, 22 South Shaoshan Road, Changsha 410000, China; liliran@csu.edu.cn (L.L.); liheng@csu.edu.cn (H.Li); 134612219@csu.edu.com (H.Lu)
* Correspondence: hzw@csu.edu.cn; Tel.: +86-731-8253-9616

Academic Editor: Andreas Sumper
Received: 2 April 2016; Accepted: 8 June 2016; Published: 13 June 2016

Abstract: Due to its fast charge and discharge rate, a supercapacitor-based energy storage system is especially suitable for power smoothing in renewable energy generation applications. Voltage equalization is essential for series-connected supercapacitors in an energy storage system, because it supports the system's sustainability and maximizes the available cell energy. In this paper, we present a high-efficiency voltage equalization scheme for supercapacitor energy storage systems in renewable generation applications. We propose an improved isolated converter topology that uses a multi-winding transformer. An improved push-pull forward circuit is applied on the primary side of the transformer. A coupling inductor is added on the primary side to allow the switches to operate under the zero-voltage switching (ZVS) condition, which reduces switching losses. The diodes in the rectifier are replaced with metal-oxide-semiconductor field-effect transistors (MOSFETs) to reduce the power dissipation of the secondary side. In order to simplify the control, we designed a controllable rectifying circuit to achieve synchronous rectifying on the secondary side of the transformer. The experimental results verified the effectiveness of the proposed design.

Keywords: voltage equalization; supercapacitor; energy storage systems; renewable generation applications

1. Introduction

In recent years, a growing interest has been seen in renewable generation systems; the most common renewable energy sources are solar and wind energy [1]. The naturally intermittent properties of wind speed and sunlight cause power fluctuations in wind turbines and photovoltaic systems, so it is difficult to store the renewable energy for future use [2]. Thus, an energy storage system (ESS) is needed in renewable generation systems to manage the power flow [3].

Conventionally, there are two popular ESSs for renewable generation systems: batteries and supercapacitors [4,5]. Batteries feature location flexibility and scalable capacity, which make them a suitable ESS technology for integration with renewable generation systems [6,7]. A major drawback of batteries is their slow dynamics. Because the power output is heavily weather dependent and changes rapidly, the battery lifetime and state-of-charge (SOC) are greatly degraded [8]. A promising new ESS technology is to use supercapacitors, which have excellent characteristics, such as a large power density, fast charge/discharge rate, high efficiency and a long cycle life [9–11].

Because of the relatively low voltage and capacity of a supercapacitor cell, hundreds of supercapacitors are typically connected in series to satisfy the large voltage and power requirements of renewable generation applications. When multiple supercapacitors are connected in series, the cell imbalance is a serious problem [12,13]. The cell imbalance of supercapacitors is typically caused by

manufacturing and environmental factors [14–16]. In an unbalanced supercapacitor ESS, cells with a small capacity may be overcharged or over-discharged during operation, which is harmful to the system [17,18]. In order to ensure the safety of the ESS while improving its efficiency, the voltage needs to be actively equalized [19].

There are many papers [20–24] concerned about the renewable energy storage system. Figure 1 shows the typical structure of the supercapacitor ESS in a renewable generation system.

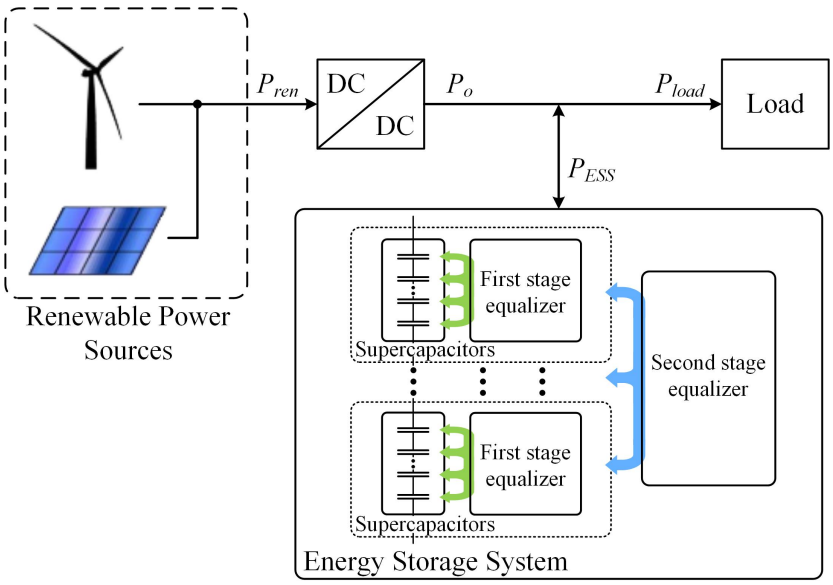

Figure 1. The structure of the supercapacitor energy storage system (ESS) in renewable generation systems.

In [20], the authors presented an original control algorithm for a hybrid energy system with a renewable energy source. A supercapacitor module functioned by supplying energy to regulate the DC-bus energy, and the fuel cell supplied energy to the supercapacitor module in order to keep it charged. The literature [21] presented a power smoothing strategy based on a supercapacitor for power conditioning of distributed renewable generation. The power smoothing controller generated the power reference for the DC/DC converter, which has a power tracking control implemented with sliding-mode techniques. In [22], the authors presented a method of improving battery lifetime in a small-scale remote-area wind-power system by the use of a battery/supercapacitor hybrid energy storage system. The supervisory control algorithm and hardware implementation were described, and the projected long-term benefits of the proposed system were assessed by simulation. In [23], a hybrid control strategy was designed and analyzed for a hybrid energy storage system (HESS). In the proposed method, batteries were used to balance the slow changing power surges, whereas supercapacitors (SC) were used to balance the fast changing power surges. In [24], the authors considered a renewable energy hybrid power plant, fed by photovoltaic (PV) and fuel cell (FC) sources with a supercapacitor (SC) storage device. They designed an intelligent fuzzy logic controller based on the flatness property for DC grid voltage regulation, and the authors proposed a simple solution to the fast response and stabilization problems in the power system.

These studies investigated different aspects of the supercapacitor energy storage system in renewable generation applications. However, they did not consider the voltage equalization of supercapacitors in the application. In fact, the voltage equalization is an important topic in supercapacitor applications.

In renewable energy applications, supercapacitors are typically divided into several modules, where each module consists of several cells connected in series [25]. The equalizer can be divided into two stages: controlling the voltage balance within the module and balancing the voltages among

modules. The first-stage and second-stage equalizers can be designed to share the same circuit topology. This modular design method can reduce the complexity and voltage stress of equalizers. Moreover, a modular supercapacitor ESS is scalable and easy to maintain [26].

In renewable generation applications, supercapacitors are usually used to deal with the quick power fluctuations [27]. Thus, the ESS is charged and discharges very rapidly [21], which places severe demands on the voltage equalizer. The system needs to supply a large equalization current to equalize the voltage in a short amount of time. Moreover, with the increased equalization current, the equalization circuit needs to be at a high level of efficiency. Hence, both the equalization rate and equalization efficiency should be considered in the design.

Generally, existing voltage equalization schemes can be divided into two categories, *i.e.*, the passive scheme and the active scheme. In the passive scheme, a resistor is connected in parallel with a supercapacitor cell to absorb the extra energy [28]. The implementation of the passive scheme is simple and inexpensive, with lower efficiency due to the involvement of lossy resistors. The passive voltage balancing schemes are usually used for low power applications.

In the active scheme, the energy is transferred among supercapacitor cells with the help of power converters. As compared to the passive circuit-based approaches, higher efficiency can be achieved in the active voltage balancing circuits, since less loss is generated by the voltage balancing circuits. There are two types of energy transfer modes, which are cell to cell mode [29] and stack to cell mode [30,31] in an active cell balancing circuit.

The stack-to-cell mode is more suitable for the supercapacitor energy storage system in renewable generation applications, as a higher equalization current can be provided. An equalizer based on an isolation voltage converter is a common equalization scheme [30,31]. However, the use of a diode rectifier circuit will generate very large energy losses in the condition of high equalization current. Therefore, they are not suited for renewable generation applications.

In this paper, we present the design of a rapid and efficient supercapacitor voltage equalization scheme for renewable energy applications. We propose an improved isolated converter topology that uses a multi-winding transformer. This topology can transfer the energy from the supercapacitor stack to weak cells in order to produce a higher equalization current and rapidly equalize the voltage of supercapacitors to satisfy the application requirements. An improved push-pull forward circuit is applied on the primary side of a transformer. A clamping capacitor is added to reduce the peaking voltage and to improve the equalization current, which eventually improve the voltage equalization rate. In order to improve the efficiency of the equalizer, a coupling inductor is added on the primary side to allow the switches to operate under the zero-voltage switching (ZVS) condition, thereby reducing switching losses. Diodes in the rectifier are replaced with metal-oxide-semiconductor field-effect transistors (MOSFETs) to reduce the power dissipation of the secondary side; this significantly improves the rectifier efficiency. In order to simplify the control, we designed a controllable rectifying circuit to achieve synchronous rectifying of the secondary side of the transformer. A prototype was built to verify the equalization performance.

The contribution of this paper is two-fold. Firstly, an improved voltage equalization circuit is designed by considering the intermittent and volatility characteristics of renewable energy systems. The proposed equalization circuit based on the ZVS push-pull forward and zero current detection (ZCD) rectifying circuit can supply a large equalization current, which can achieve the rapid voltage equalization of supercapacitors. Secondly, the previous equalization schemes suffer a large power loss in rectifying diodes with heavy current. We propose a controllable rectifying circuit with MOSFETs to reduce the power dissipation of the secondary side. A coupling inductor is added on the primary side, which allows the switches to operate under the zero-voltage switching (ZVS) condition to reduce switching losses. All improvements are helpful to improve the energy transfer efficiency.

The rest of this paper is organized as follows. Section 2 introduces the principle and control strategy. Section 3 gives the scheme and experiments of the equalizer. We conclude the paper in Section 4.

2. Voltage Equalizer Design

2.1. Schematic

Figure 2 shows the proposed voltage equalizer circuit, where $C_1, C_2, ..., C_n$ is n series supercapacitors in a stack and I_{ch} is the terminal current. When supercapacitors are being charged by renewable sources, I_{ch} is positive; when supercapacitors are discharging, I_{ch} is negative.

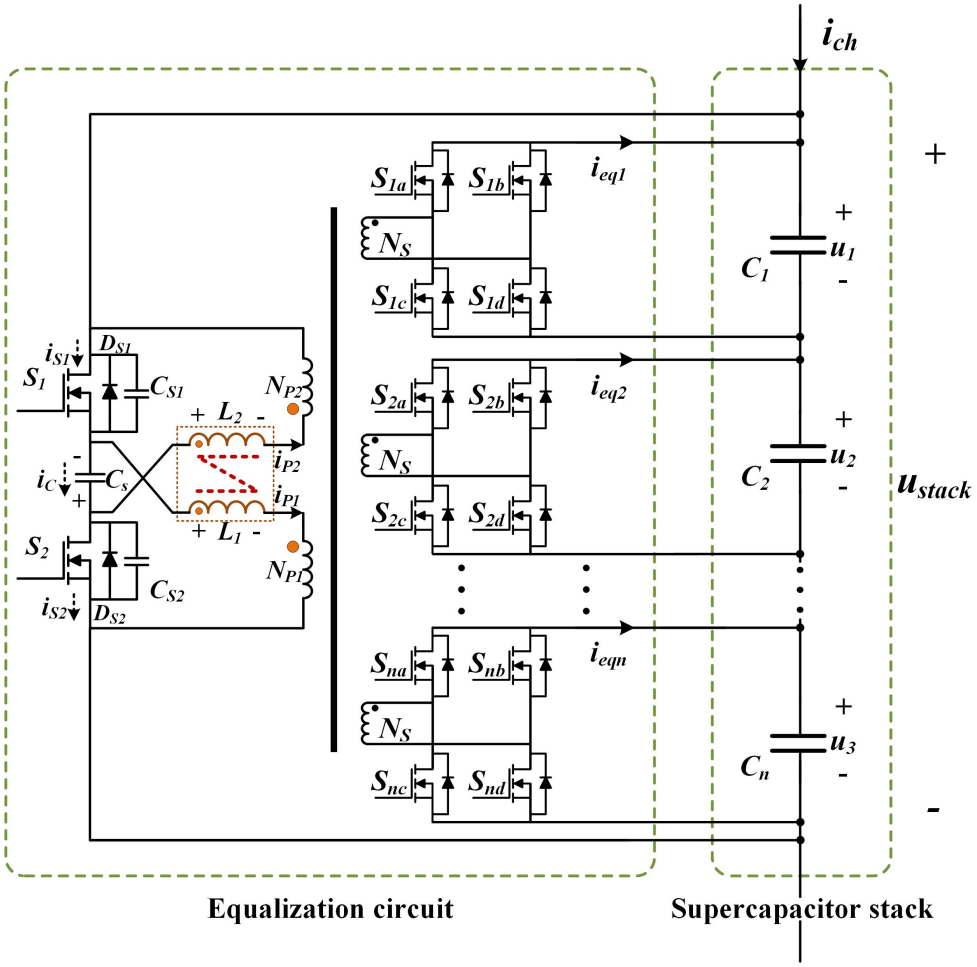

Figure 2. The proposed voltage equalization circuit schematic.

An improved push-pull forward topology with clamping capacitors is used on the primary side of the transformer. The input voltage of the converter is used as the voltage of the supercapacitor stack. The improved push-pull forward topology adds a clamping capacitor to the traditional push-pull converter. This clamping capacitor can absorb the energy of the leakage inductance and feedback to the input, so the peak voltage can be constrained when the main switches S_1, S_2 turn off and the switch requirement is lowered. Applying clamping capacitors couples the two windings of the primary side. When the equalizer is working, the two windings of the primary side transmit energy to the secondary side at the same time. In other words, two forward converters transmit energy to the secondary side in parallel to increase the output current of the equalization circuit. By adding the coupling inductances L_1 and L_2 to the primary side, the switches of the primary side are turned on under the ZVS condition, which decreases the switching loss.

The secondary side of the transformer consists of n identical controllable synchronous rectifiers. The output side of each rectifier is connected with a supercapacitor cell. The rectifier uses MOSFETs

with low internal resistance to replace the ordinary rectifier diodes. This increases the equalization current and decreases the loss of the rectifier.

For the sake of simplicity, the following assumptions were made.

(1) There are n supercapacitor cells in a stack, where the cell capacitance is $C_k(k = 1, 2, ..., n)$ and the cell voltage is $u_k(k = 1, 2, ..., n)$. The stack voltage u_{stack} is constant within a single switching period.

(2) The turn ratio of the multi-winding transformer is $K = N_p/N_s$. The multi-winding transformer has two primary windings, where $N_{p_1} = N_{p_2} = N_p$, and n secondary windings, where $N_{sk} = N_s\ (k = 1, 2, \ldots, n)$. The magnetizing inductance and leakage inductance of the transformer are ignored.

(3) The coupled inductors comprise L_1 and L_2. The equivalent inductance of coupled inductors is $L_{eq} = L + M$, where L is the self-inductance of the inductors and M is the mutual inductance between L_1 and L_2. The equivalent inductances of L_1 and L_2 are equal, where $L_{eq} = L_{eq1} = L_{eq2}$.

(4) The voltage of the clamp capacitor C_s is equal to the stack voltage u_{stack} in the steady state.

(5) The switches and diodes are ideal.

Figure 3 shows key waveforms of the proposed equalization circuit in the steady state, where V_{gs} are the corresponding driving signals of S_1 and S_2, V_{ds1} is the drain-source voltage of S_1, V_{ds2} is the drain-source voltage of S_2, V_{L_1} is the voltage across the inductor L_1, V_{L_2} is the voltage across the inductor L_2, i_{p1} and i_{p2} are the winding currents of the transformer on the primary side and i_{eq} is the equalization current supplied to the supercapacitor cell.

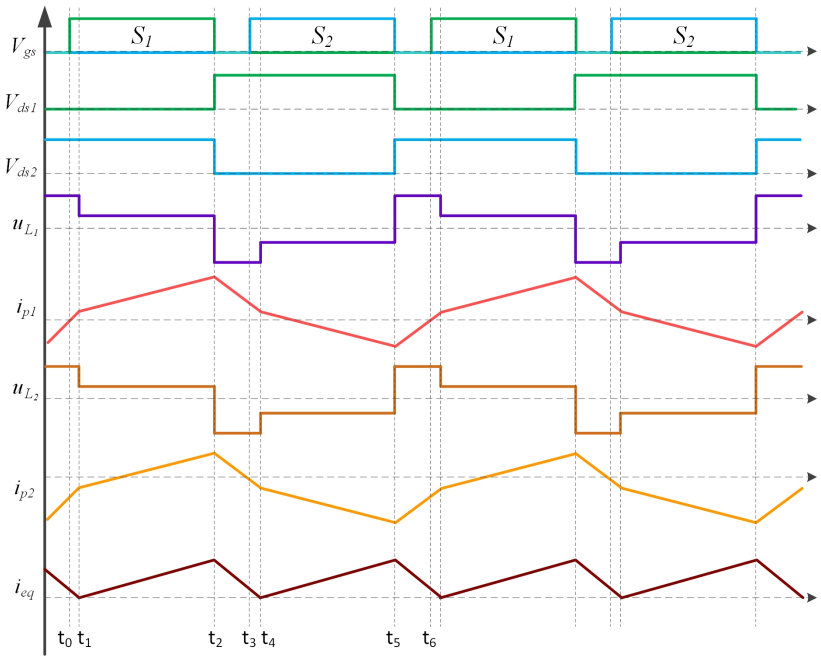

Figure 3. Key waveforms of the proposed voltage equalization circuit.

Suppose that the supercapacitor C_1 is the cell with the lowest voltage and that the rectification circuit connected to C_1 works first. There are six modes within one switching period. Figure 4 shows the equivalent circuit of each mode.

Mode 1 ($t_0 - t_1$; Figure 4a): Before t_0, the body diode of the switch S_1 is still conducting. The voltage across S_1 is nearly zero. At t_0, the switch S_1 is turned on under the zero-voltage condition. The body diode of the switch S_1 turns off. The energy stored in the leakage inductor of the winding N_{p2} is released to the clamping capacitor through S_1, while the energy stored in the leakage inductor of the winding N_{p1} is released to the supercapacitor stack. The primary current i_{p1} flows through the path $U_{stack-} \rightarrow N_{p1} \rightarrow L_1 \rightarrow S_1 \rightarrow U_{stack+}$, and i_{p2} flows through the path $V_{C_s-} \rightarrow S_1 \rightarrow N_{p2} \rightarrow L_2 \rightarrow V_{C_s+}$. S_{1b} and S_{1c} remain on.

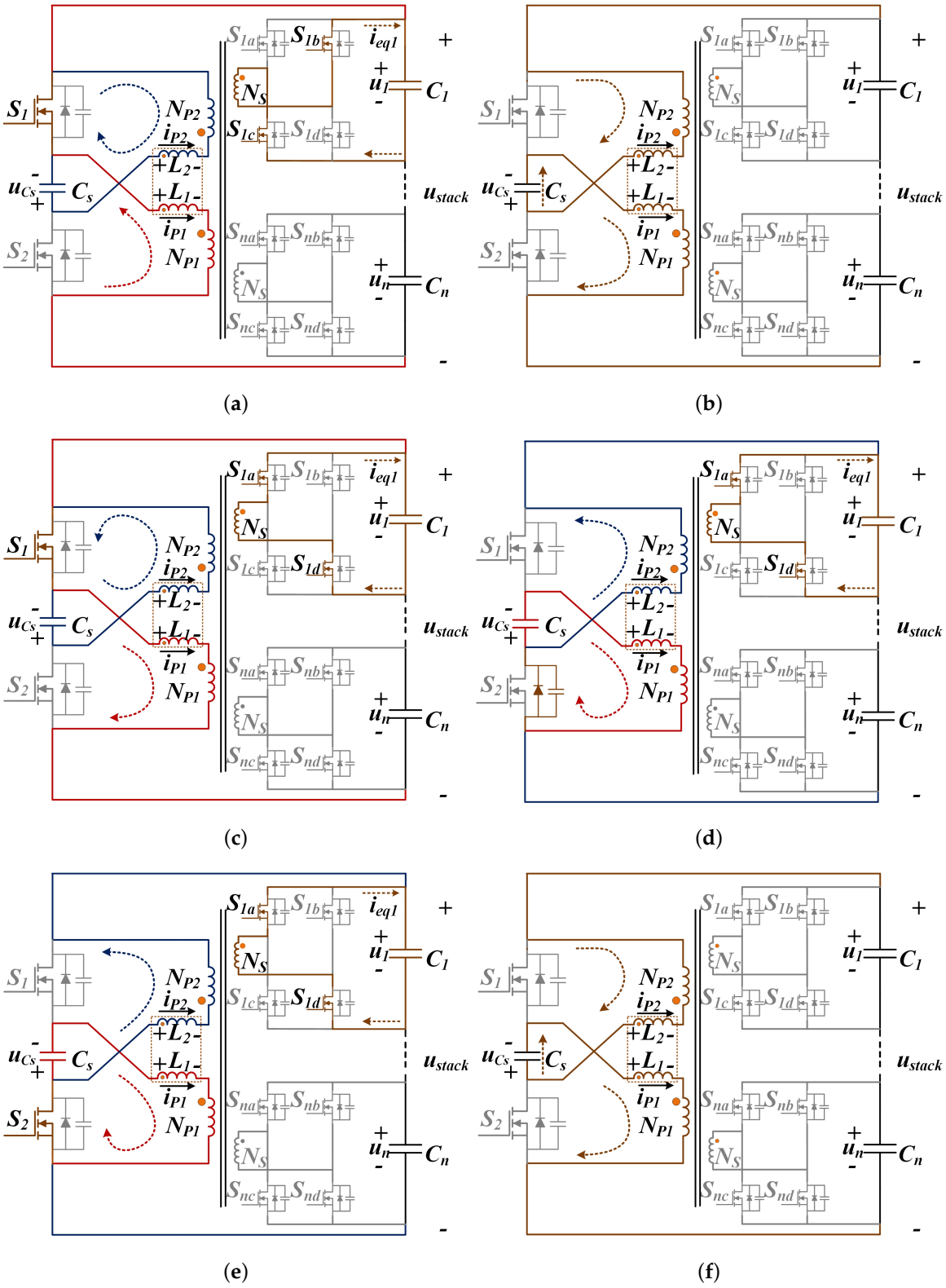

Figure 4. *Cont.*

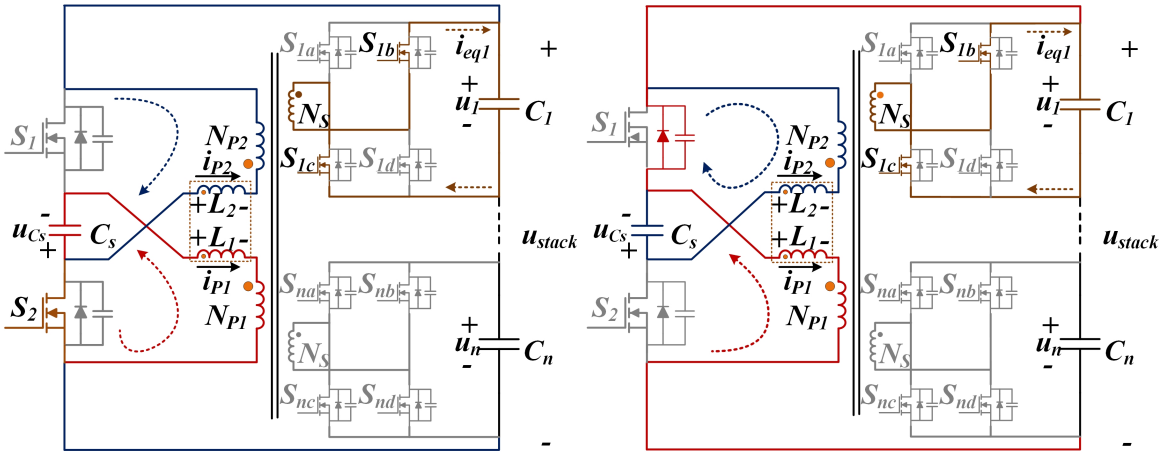

Figure 4. The operation modes of the equalizer circuit. (**a**) Mode 1: $t_0 < t < t_1$; (**b**) time t_1; (**c**) Mode 2: $t_1 < t < t_2$; (**d**) Mode 3: $t_2 < t < t_3$; (**e**) Mode 4: $t_3 < t < t_4$; (**f**) time t_4; (**g**) Mode 5: $t_4 < t < t_5$; (**h**) Mode 6: $t_5 < t < t_6$.

The corresponding currents can be calculated as follows:

$$\begin{cases} i_{p1}(t) = i_{p1}(t_0) + \dfrac{u_{stack} + K \cdot u_1}{L_{eq}}(t - t_0); \\ i_{p2}(t) = i_{p2}(t_0) + \dfrac{u_{C_s} + K \cdot u_1}{L_{eq}}(t - t_0); \end{cases} ; t \in [t_0, t_1] \quad (1)$$

During this process, the balancing current i_{eq1} drops to zero when $i_{p1} = -i_{p2}$. S_{1b} and S_{1c} are turned off at t_1.

Mode 2 ($t_1 - t_2$: Figure 4c): As shown in Figure 4b, the primary current is $i_{p1} = -i_{p2}$ at time t_1. At this point, the current through S_1 is zero. The primary windings of the transformer are connected in series with the clamping capacitor. The primary current flows through the path $U_{stack+} \rightarrow N_{p2} \rightarrow C_s \rightarrow N_{p1} \rightarrow U_{stack-}$. It is called the circulating current I_a, where $I_a = i_{p1} = -i_{p2}$.

After the time t_1, the stack voltage and clamping capacitor voltage are added to the primary windings N_{p1} and N_{p2}, respectively. The current i_{p1} increases linearly. The current i_{p2} changes from negative to positive. Energy is transferred to the secondary side.

The secondary winding N_{S1} generates an induced voltage. The switches S_{1a} and S_{1d} turn on quickly. The equalization current of the secondary side i_{eq} increases and charges the supercapacitor C_1.

When the switches S_{1a} and S_{1d} turn on, the voltage of the secondary side is clamped at the voltage u_1. Because the turn ratio of the transformer is K, the voltage of the two primary windings is Ku_1.

The current flowing through the primary windings is given by:

$$\begin{cases} i_{p1}(t) = I_a + \dfrac{u_{stack} - K \cdot u_1}{L_{eq}}(t - t_1); \\ i_{p2}(t) = -I_a + \dfrac{u_{C_s} - K \cdot u_1}{L_{eq}}(t - t_1); \end{cases} ; t \in [t_1, t_2] \quad (2)$$

At the time t_2, the equalization current of the secondary side i_{eq} reaches its maximum $i_{eq\,\max}$:

$$i_{eqmax} = 2K\left(u_{stack} - K \cdot u_1\right) \cdot \left(t_2 - t_1\right) / L_{eq} \quad (3)$$

Mode 3 ($t_2 - t_3$: Figure 4d): This figure shows the circuit working state in Mode 3. At the time t_2, S_1 turns off and S_{1a} and S_{1d} stay on. Then, the inductances L_1 and L_2 generate a reverse induced

voltage, and S_2 turns on. The leakage energy of the coupled inductor L_1 is absorbed by the clamping capacitor. The coupled inductor L_2 also releases leakage energy to the supercapacitor stack through S_2. Meanwhile, the current i_{p1} of the primary windings decreases quickly, and i_{p2} decreases to zero and then reverses to quickly increase. The equalization current of the secondary side i_{eq} decreases quickly.

During this process, the current flow though the two primary windings is given by:

$$\begin{cases} i_{p1}(t) = i_{p1}(t_2) - \dfrac{u_{C_s} + K \cdot u_1}{L_k}(t - t_2); \\ i_{p2}(t) = i_{p2}(t_2) - \dfrac{u_{stack} + K \cdot u_1}{L_k}(t - t_2); \end{cases} ; t \in [t_2, t_3] \quad (4)$$

At the time t_3, the switch S_2 turns on. Modes 4–6 are similar to Modes 1–3, so their description is omitted here.

2.2. Controllable Rectifier Circuit

In order to achieve rapid equalization, the equalization current through the transformer's secondary side becomes very large. Because diode-based rectifiers produce very high heat loss, we decided to replace the diodes with low on-resistance MOSFETs to effectively improve the rectifier efficiency.

In order to satisfy the operation requirements of a supercapacitor equalizing system, we chose MOSFET IRFS7434-7PPBF designed by IR Company. The on-resistance is about 0.7 mΩ with a maximum value of 1 mΩ. The leakage current is as much as 240 A. Figure 5 shows a schematic of the proposed rectifier.

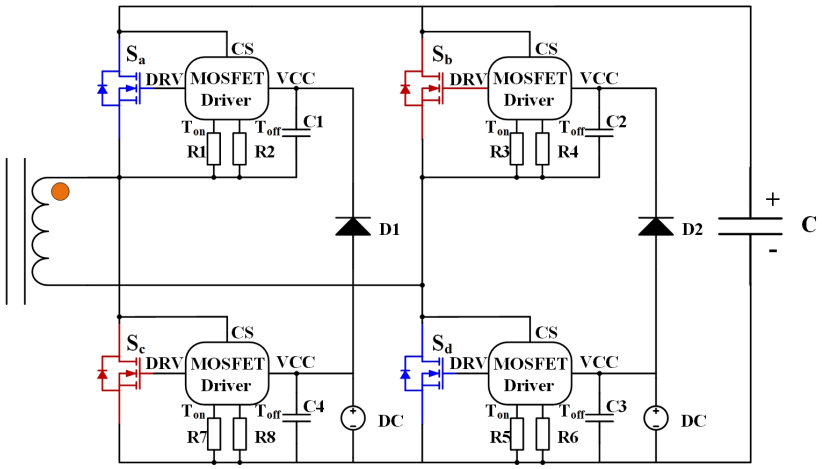

Figure 5. The schematic of the controllable rectifier.

Figure 6 describes the circuit architecture of the MOSFET driver. The proposed MOSFET driver features a high current gate driver along with high-speed logic circuitry to provide appropriately-timed drive signals to a MOSFET for synchronous rectification. Zero-current detection (ZCD) is applied to reduce the power loss of the parasitic diode. Once the current flowing through the MOSFET is detected, the MOSFET turns on; this efficiently avoids parasitic diode conductance.

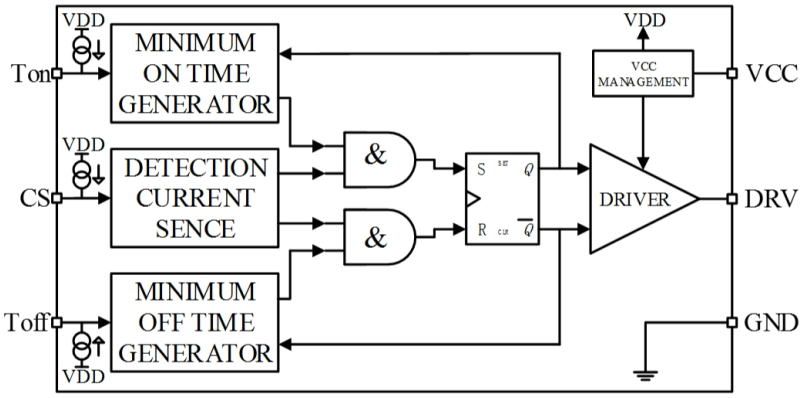

Figure 6. The structure of the MOSFET driver.

2.3. Voltage Equalization Control Algorithm

The proposed equalizing scheme involves transferring energy from the supercapacitor stack to cells with low voltage. Then, the voltages among supercapacitors can be equalized. A controller measures the voltages of cells and computes the maximal voltage difference among supercapacitors. If the lowest voltage is u_i and the highest voltage is u_j, Δu_{ij} represents the voltage difference between the j-th and i-th supercapacitor cell, *i.e.*, $\Delta u_{ij} = u_j - u_i$. When Δu_{ij} is larger than a small threshold u^*, the corresponding rectifier connected to the i-th supercapacitor cell is enabled, and an equalizing current is supplied to the i-th cell, which transfers energy from other cells to the i-th cell. At the same time, the voltages of other cells decrease because of the energy transfer.

Because the equalization current is very large, the voltage drop for the equivalent resistance of the supercapacitor is large. Then, the terminal voltage u_i cannot accurately represent the capacitor voltage when the supercapacitor is charged with the equalization current. In order to avoid this shortcoming, we adopted a pulse equalizing method, *i.e.*, the equalizer only works for a small duration and then stops until the current ripples disappear. The equalizer then measures the voltage of the supercapacitors again and starts the next equalization cycle.

Note that there is noise in the voltage measurements. Thus, it is difficult to ensure that all supercapacitor voltages are completely the same. When all of the supercapacitor voltage differences are within the threshold u^*, the voltages are considered to be equalized. The voltage equalization control algorithm is as follows:

Algorithm 1: Voltage equalization control

1: Initialization.
2: Measure the voltages of all supercapacitors.
3: Find the highest voltage cell j and lowest voltage cell i.
4: Calculated the voltage difference between u_i and u_j: $\Delta u_{ij} = u_j - u_i$.
5: If $\Delta u_{ij} > u^*$, then
6: Enable the i-th rectifier.
7: Enable the remaining rectifier for a short time.
8: Disable the i-th rectifier.
9: End if.
10: Go to step 2.
11: End.

3. Implementation and Experimental Results

In this section, we introduce the implementation of the voltage equalizer for supercapacitors. The experiment setup is shown in Figure 7. Figure 7a shows the voltage equalizer test bench that is comprised of eight parts: a control board, a push-pull forward converter, a multi-winding transformer,

eight controlled rectifiers, a current measure board, a supercapacitor stack, a discharge load and a current charger. Figure 7b shows the controlled rectifier, which is the fourth part in Figure 7a. Figure 7c shows the control board, which is the first part in Figure 7a.

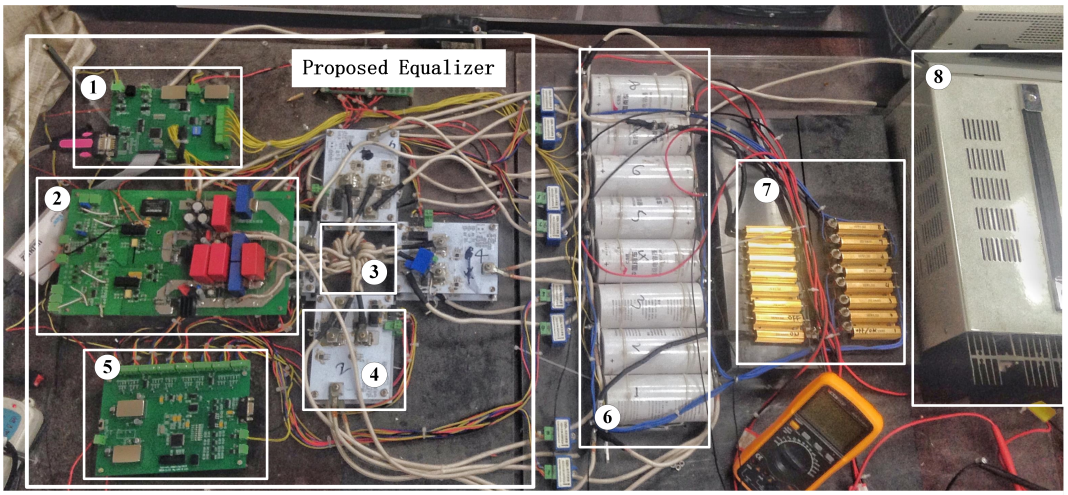

① Control Board; ② Push-pull forward converter; ③ Multi-winding transformer; ④ Controlled rectifier; ⑤ Current measure board; ⑥ Supercapacitor stack; ⑦ Discharge load; ⑧ Current charger;

(**a**)

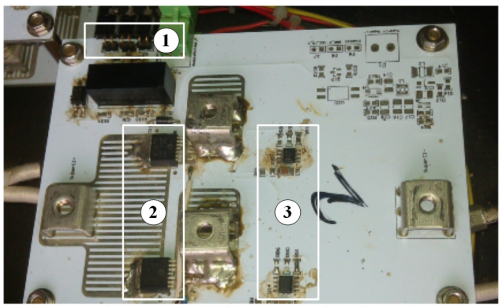

① Control port; ② MOSFETs; ③ MOSFET Driver

(**b**)

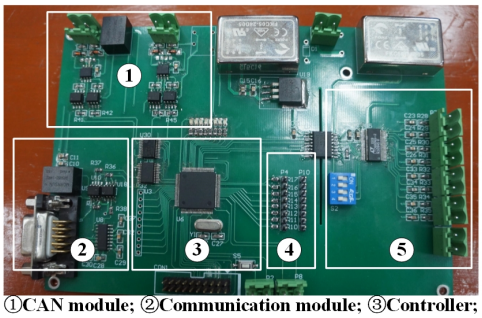

①CAN module; ②Communication module; ③Controller; ④ Control port; ⑤ Voltage measure module

(**c**)

Figure 7. The experiment setup. (**a**) Voltage equalizer test bench; (**b**) controlled rectifier; (**c**) control board.

As shown in Figure 7a, the hardware components of the proposed equalizer were divided into five parts: control board, push-pull forward converter, multi-winding transformer, controlled rectifiers and current measure board. The control board measured the terminal voltage of each supercapacitor cell and regulated the equalization circuit based on these measurements. The current measure board was used to measure and record the equalization current. The supercapacitor stack was connected with the equalizer and could be charged by the current charger and discharged through the discharge load, which was used to imitate the charging and discharging process of renewable energy storage systems. In what follows, we will introduce these components in detail.

Supercapacitor stack: The supercapacitor stack consisted of eight series supercapacitors. Each supercapacitor had a rated voltage of 2.7 V and a rated capacity of 3000 F.

Push-pull forward converter: The push-pull forward converter was the main power circuit of the voltage equalizer. The input of the push-pull forward converter was connected to the supercapacitor stack. The output of the push-pull forward converter was connected to a multi-winding transformer. During the equalization process, energy was transferred along the following path: stack → push-pull

forward converter → transformer → rectifier → supercapacitor cell. In the experiment, the duty cycles of switches S_1 and S_2 were 0.5, *i.e.*, the two switches were turned on alternately.

Multi-winding transformer: The multi-winding transformer was mainly used for the energy transfer and used to maintain electrical isolation among rectifiers. The multi-winding transformer had two primary windings and eight secondary windings. The primary winding was connected to the push-pull forward converter. Each secondary winding was connected to a rectifier circuit. A toroidal core was used to simplify the transformer outgoing line design.

Controlled rectifier: As shown in Figure 7b, controlled rectifiers were used to convert the alternating current to a direct current. There were eight controlled rectifiers in the voltage equalizer. Each rectifier connected one secondary winding of the transformer and one supercapacitor cell. The rectifier circuit could reach dozens of amperes and even hundreds of amperes. In order to ensure a good cooling effect and increase system reliability, the rectifier circuit was formed on the base of a double-sided aluminum substrate.

The MOSFET driver was used to control the switching on or switching off of MOSFETs of the rectifier. The control port of the control board was connected to the control port of the rectifier. The control board could enable or disable the rectifier with a control signal through the control ports. The control board determined if the rectifier needed to be enabled. When the rectifier was enabled, the energy flowed into the corresponding supercapacitor.

Control board: As shown in Figure 7c, the control board was the core of the voltage equalizer. The control board was used to measure all supercapacitor voltages and to control the rectifiers. The control board consisted of a voltage measurement module, controller, communication module, CAN module and control port. The voltage measurement module used a high-precision voltage sampling chip to measure all supercapacitor voltages. A LPC1768 microcontroller was used as the controller to run the algorithm. The communication module was used to communicate with the computer. All supercapacitor voltage data were transmitted to the PC. The CAN module was mainly used for inter-module communication and data exchange between primary and secondary equalizers. In the experiment, the CAN module worked as the communication interface between the control board and current measure board. The control ports were connected to the rectifier boards. The control board determined which rectifier needed to be enabled based on the result of the control algorithm.

Current measure board: The current measure board was used to measure the equalization currents. There is a current sensor between each rectifier and the corresponding supercapacitor cell. The current measure board transmitted the sensor data to the control board through CAN module.

Current charger: The current charger was used to charge the supercapacitors. The charging process of supercapacitors with renewable energy sources, such as solar and wind energy, can be simulated by controlling the output current of the charger.

Discharge load: The discharge load was the load of the supercapacitors and was used to emulate the discharge process of supercapacitors. The discharge load was a 1.6 Ω resistor connected with the supercapacitor stack in parallel. The supercapacitor stack could discharge through the resistor load, which could emulate the discharging process.

Figure 8 shows the switching transitions of switches S_1, S_{1a} and S_{1b} when the controller enabled the first rectifier. V_{gs1} is the gate-source voltage of switch S_1, and V_{gs1a} and V_{gs1b} are the gate-source voltages of switches S_{1a} and S_{1b}. When S_1 was on (V_{gs1} was 15 V), the rectifier ensured that S_{1a} (S_{1d}) was on and S_{1b} (S_{1c}) was off. Otherwise, when S_2 was on, *i.e.*, S_1 was off, S_{1b} (S_{1c}) was on and S_{1a} (S_{1d}) was off. Figure 8 shows the whole process.

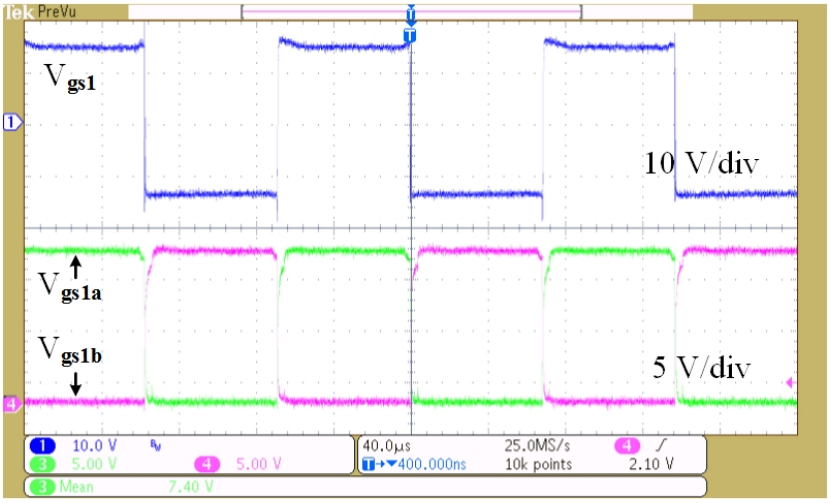

Figure 8. Switching transitions of switches S_1, S_{1a} and S_{1b}.

Figure 9 shows the secondary side current of the transformer. V_{gs2} is the gate-source voltage of switch S_2. I_{sec} is the measured secondary side current of the transformer. Because S_1 and S_2 were turned on alternately, the durations of Mode 3 (t_2-t_3) and Mode 6 (t_5-t_6) were approximately zero. Based on the theoretical analysis in Section 2, when S_2 was off and S_1 was on, the leakage current of the primary side was fed back to the supercapacitor stack and clamping capacitor. The secondary side current rapidly decreased to zero. From t_1, the supercapacitor stack and clamping capacitor supplied energy to the secondary side, and the secondary side current increased. S_1 was off, and S_2 was on at t_2; the secondary side current rapidly decreased to zero and then increased. Thus, the experimental results conformed well to the theoretical analysis.

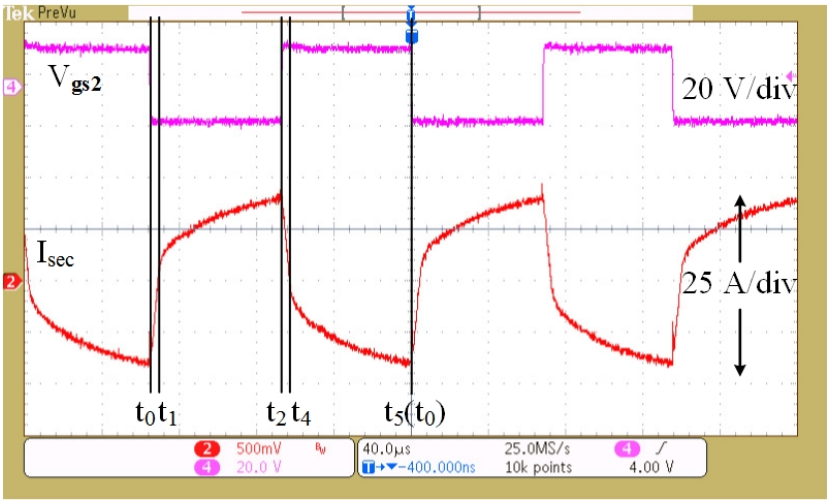

Figure 9. The current through secondary side of the transformer in equalization.

Figure 10 shows the equalization current from the equalization circuit to the supercapacitor cell during the equalization process. V_{gs1} is the gate-source voltage of the switch S_1. I_{eq} is the measured equalization current. The average equalization current was 60 A, which satisfies the requirements of renewable energy applications.

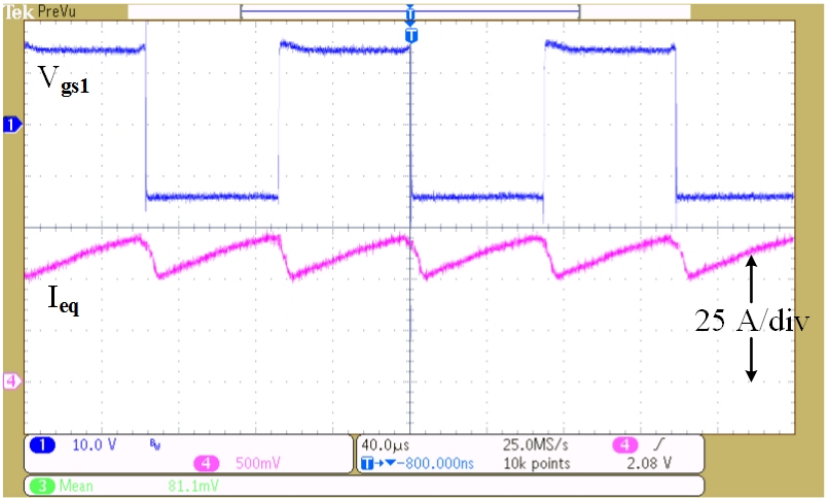

Figure 10. The equalization current supplied to the supercapacitor cell in the equalization process.

The performance of the proposed voltage equalizer is evaluated under three different operating conditions.

- Case I. All supercapacitor cells have different initial voltage values and are charged with a 10-A constant current source.
- Case II. All supercapacitor cells have different initial voltage values and discharge through connecting a 1.6 Ω resistor in parallel.
- Case III. All cells have different initial voltage values without charging and discharging.

The initial voltage of supercapacitor cells in different operating conditions is shown in the Table 1.

Table 1. The initial voltage of supercapacitor cells.

The Voltage of Cells	Case I	Case II	Case III
V_{C_1}	1.693 V	1.749 V	1.814 V
V_{C_2}	1.677 V	1.762 V	1.810 V
V_{C_3}	1.682 V	1.761 V	1.820 V
V_{C_4}	1.602 V	1.698 V	1.658 V
V_{C_5}	1.702 V	1.766 V	1.833 V
V_{C_6}	1.672 V	1.783 V	1.815 V
V_{C_7}	1.673 V	1.742 V	1.767 V
V_{C_8}	1.517 V	1.639 V	1.606 V
Maximum Difference	0.185 V	0.144 V	0.227 V

In order to emulate the supercapacitor charging process with renewable energy sources, a current charger was applied to charge the supercapacitors. The charging current was set to 10 A. Figure 11a shows the voltage curve of the supercapacitors during charging. The initial voltages of the eight cells were 1.693, 1.677, 1.682, 1.602, 1.702, 1.672, 1.673 and 1.517 V. The maximum initial voltage difference was 185 mV. Because C_8 had the lowest voltage, the control board enabled the corresponding rectifier, and the equalizer then supplied current to C_8. The voltage of C_8 increased rapidly. When the voltage of C_8 was equal to C_4 (*i.e.*, this had the second-lowest voltage), the voltages of the two supercapacitor cells increased alternately. This process repeated until the voltages of all cells were equalized. In practical applications, the measurement noise made precise equalization impossible. Thus, when the maximum voltage difference was less than 20 mV, the cells were assumed to have the same voltages. The first equalization was achieved at 28 s. During the charging process, the rates of increase in the

cell voltages differed owing to the individual cell capacities. When the voltage difference was larger than 20 mV, the equalizer worked to equalize the cell voltages. When the charging process was over, the maximum voltage difference was 20 mV.

The equivalent circuit of the supercapacitors contained an internal resistance. When the equalizer worked, the equalizing current was large, the resistor voltage was large and the terminal voltage could no longer be treated as the cell voltage. Figure 11b shows the equalization current i_{eq} of each cell. The equalization current of C_8 could be as high as 54 A, which resulted in an abrupt terminal voltage increase. Though the practical voltage of C_8 was the lowest, the terminal voltage of C_8 was the highest. In the experiment, a pulse equalizing scheme was applied to mitigate the internal resistance effect.

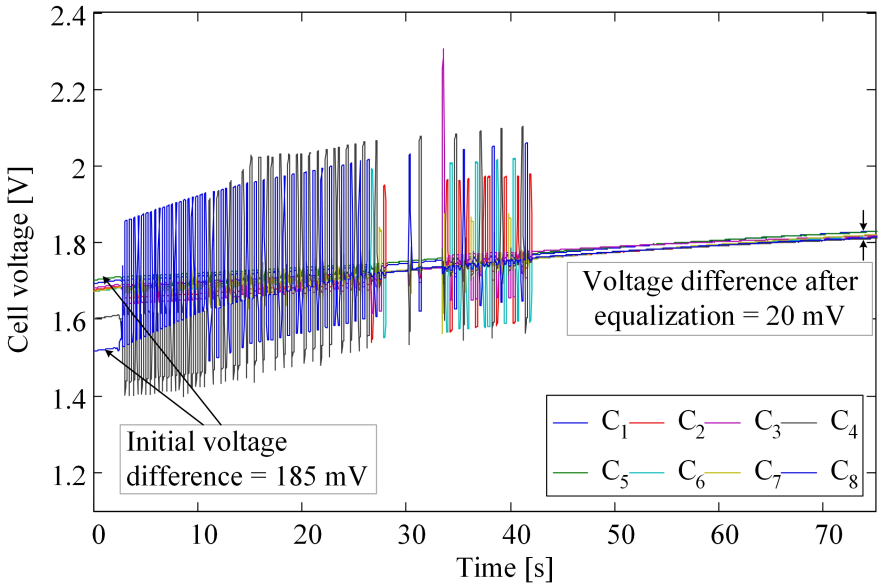

(**a**)

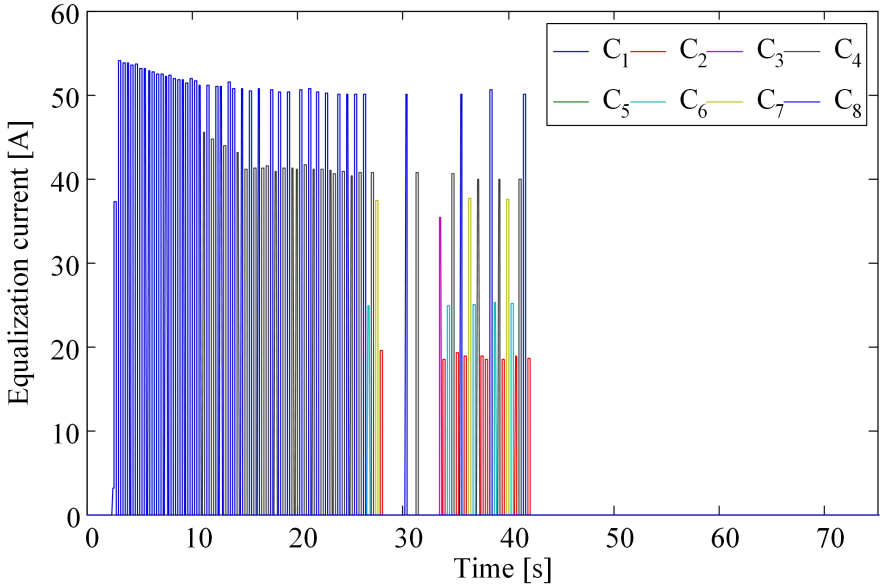

(**b**)

Figure 11. The voltage charging process. (**a**) The cell voltage profiles; (**b**) the equalization current profiles.

In order to emulate the discharging process of supercapacitor modules, supercapacitors were discharged with parallel resistors. Figure 12a shows the voltage curve during discharge. The initial voltage difference was 144 mV. Similar to the charging process, the voltage of the cell with the lowest voltage increased rapidly, and the voltages of the other cells decreased rapidly until equalization was achieved. Figure 12b shows the equalization current of cells during the discharging process.

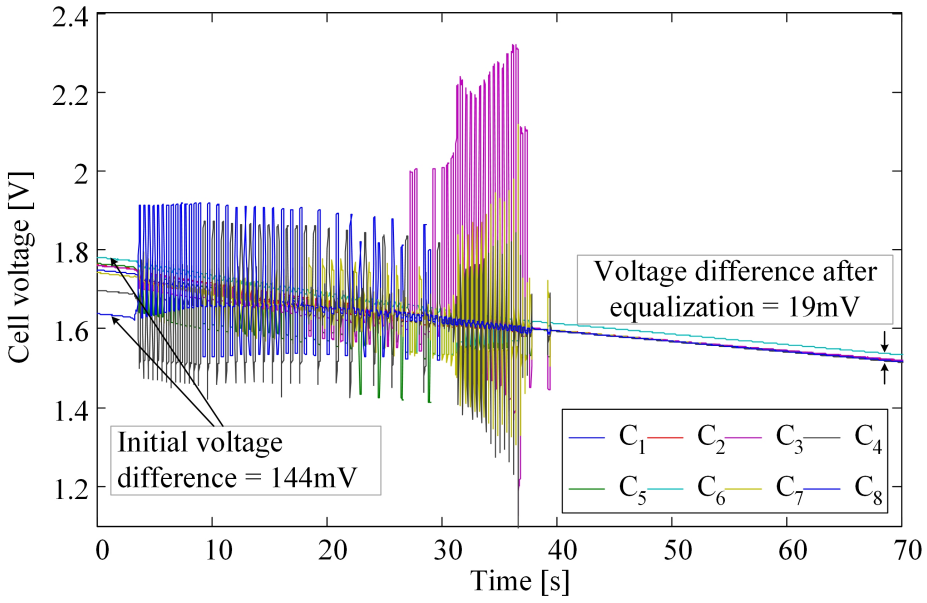

(**a**)

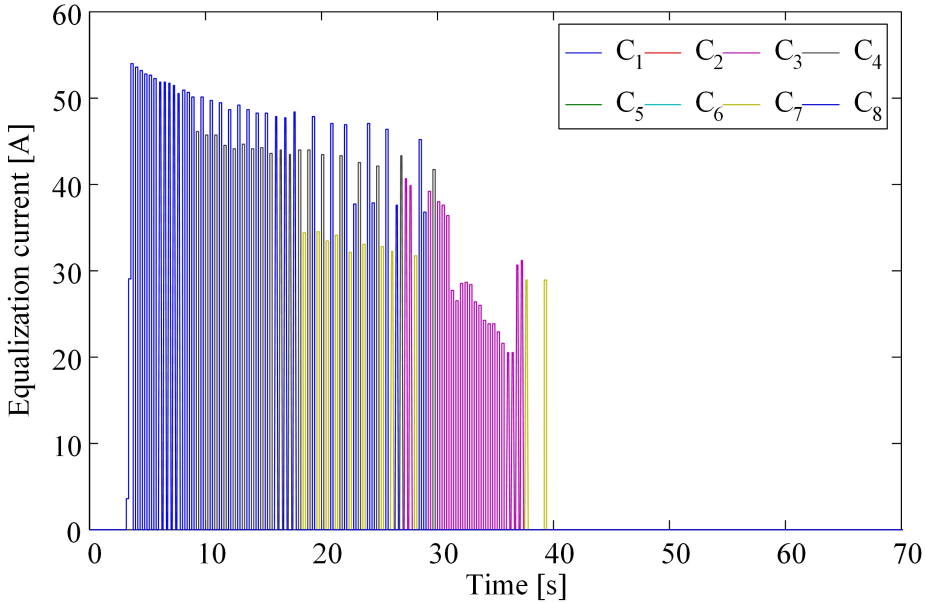

(**b**)

Figure 12. The voltage discharging process. (**a**) The cell voltage profiles; (**b**) the equalization current profiles.

Figure 13 presents the equalization process during steady state, *i.e.*, there are no charging or discharging operations for supercapacitor energy storage systems. This case can happen when there are no power sources (e.g., no wind or no sunlight) and no loads of supercapacitors.

The initial voltage difference was set to 227 mV. After about 40 s, all cells' voltages reached equilibrium. The maximal voltage difference was 19 mV after equalization. Figure 13a presents the voltage curves of supercapacitor cells, and Figure 13b presents the equalization current through supercapacitor cells during equalization. From Figure 13b, it can be seen that the maximal equalization current could reach to 60 A. With the equalization process, the cell voltage increased and the equalization current decreased gradually. Because there exist differences in the equivalent inter-resistances and equivalent resistances among different supercapacitor cells and different rectifiers, the equalization currents were different. More total resistance leads to less output equalization current.

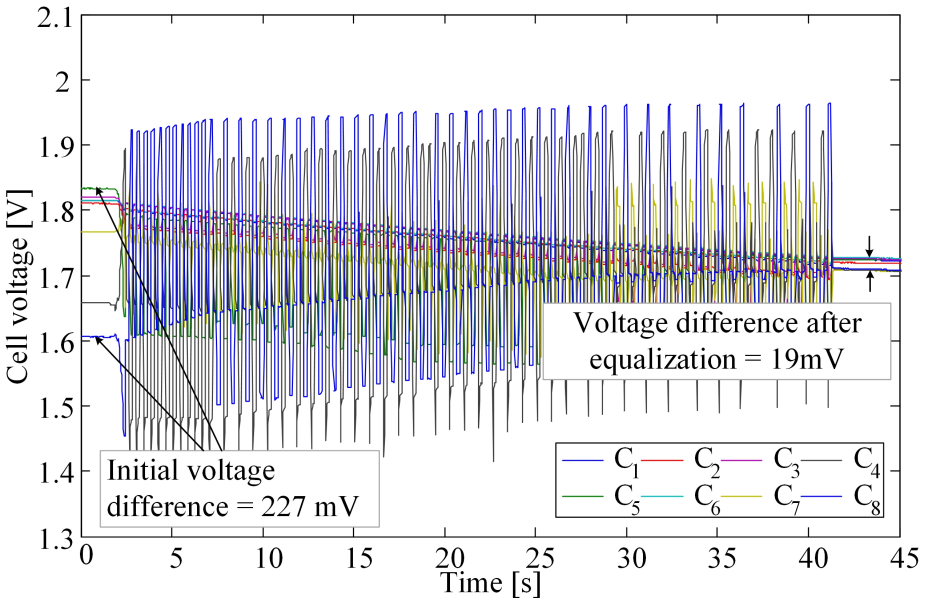

(**a**)

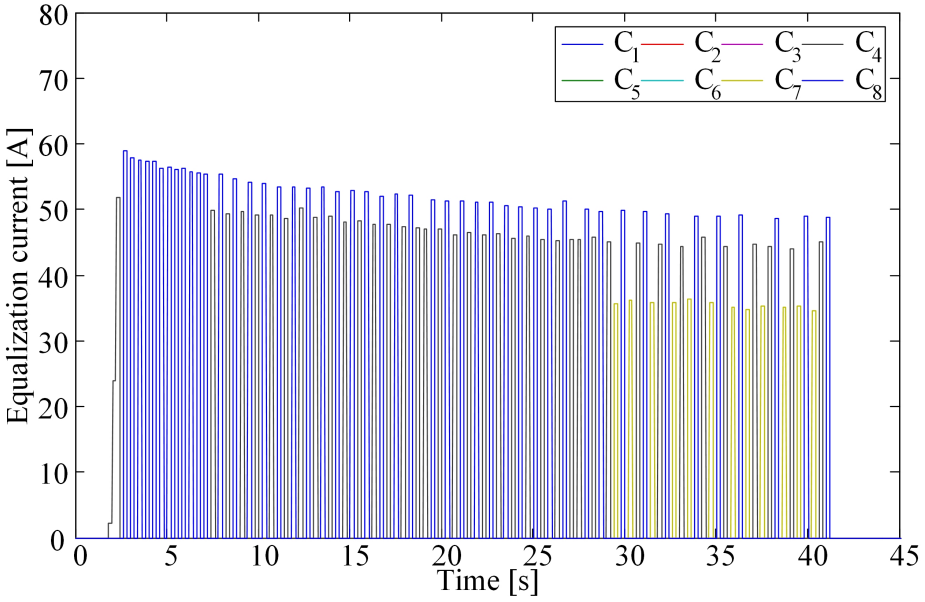

(**b**)

Figure 13. The voltage equalization process. (**a**) The cell voltage profiles; (**b**) the equalization current profiles.

The efficiency of the equalization circuit could be obtained by calculating the ratio of output power and input power. For convenience, the 15-V constant voltage power supply was adapted to replace the supercapacitor stack as the input of the equalization system. At the same time, the rectifier circuit can be controlled to ensure only one supercapacitor cell participated in the voltage equalization operation during the steady state. Figure 14 presents the transfer efficiency under different equalization currents, which are obtained from a practical test.

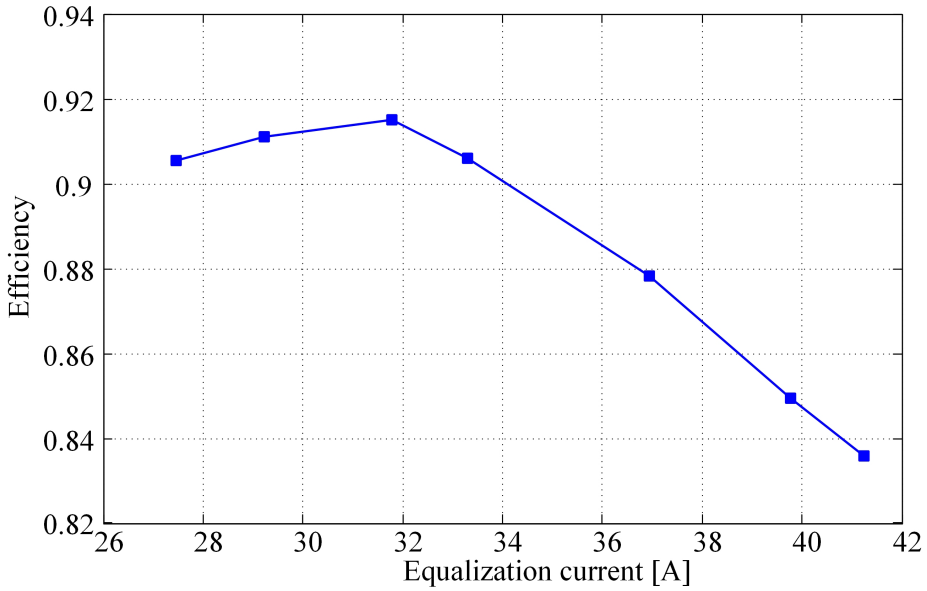

Figure 14. The transfer efficiency under different equalization currents.

From Figure 14, it is seen that the highest transfer efficiency of the proposed equalization scheme approaches 92%. With the increase of equalizing current, the system efficiency decreased. When the output current is 41 A, the system efficiency is 83%. The reason is that when output current increased, the energy loss of the secondary rectifier circuit was proportional to the square of the current.

As traditional rectifier diodes work with 0.7 V or a higher forward voltage drop, the conduction power loss of a single diode will reach 28 W when the equalization current is 40 A. This energy loss is unacceptable. In this paper, traditional diodes are replaced with MOSFET IRFS7434-7PPBF. The breakover resistance is about 0.7 mΩ with a maximum value of 1 mΩ. Therefore, the conduction power loss of a single MOSFET will be less than 1.6 W when the equalization current reaches 40 A. The power loss of the secondary side rectifier circuit is greatly reduced. In addition, there is a certain equivalent resistance between the rectifier circuit and each supercapacitor cell.

When the system is deployed in the experiment, the MOSFETs with low breakover resistance should be selected for secondary side rectifier circuit. Additionally, the wires between rectifier circuit and supercapacitors need to be shortened as much as possible to reduce the energy loss on output wires.

4. Conclusions

In this paper, we present a high-efficiency voltage equalization scheme for supercapacitor energy storage systems in renewable generation applications. We propose an improved isolated converter topology that uses a multiple-winding transformer. An improved push-pull forward circuit is applied on the primary side of the transformer. A clamping capacitor is added to reduce the peaking voltage and to improve the equalization current to eventually improve the voltage equalization rate. A coupling inductor is added on the primary side for ZVS and to reduce the switching loss. The diodes in the rectifier are replaced with MOSFETs to reduce the power dissipation of the secondary side. In order to

accurately equalize the voltages of the supercapacitors, a simple pulse equalizing method is proposed. The experimental results verified the high efficiency of the proposed equalizing scheme.

Acknowledgments: This work was partially supported by the National Nature Science Foundation (Grant Nos. 61202342, 61379111, 61402538, 61403424, 61502055).

Author Contributions: The voltage equalization circuit schematic was proposed by Zhiwu Huang. The experiment results were collected and analyzed by Liran Li and Honghai Lu. The paper was written by Liran Li and Heng Li.

Conflicts of Interest: The authors declare no conflict of interest.

References

1. Baek, S.; Park, E.; Kim, M.G.; Kwon, S.J.; Kim, K.J.; Ohm, J.Y.; Del Pobil, A.P. Optimal renewable power generation systems for Busan metropolitan city in South Korea. *Renew. Energy* **2016**, *88*, 517–525.
2. Benyahia, N.; Denoun, H.; Zaouia, M.; Tamalouzt, S.; Bouheraoua, M.; Benamrouche, N.; Rekioua, T.; Haddad, S. Characterization and control of supercapacitors bank for stand-alone photovoltaic energy. *Energy Proced.* **2013**, *42*, 539–548.
3. Mahlia, T.; Saktisahdan, T.J.; Jannifar, A.; Hasan, M.H.; Matseelar, H. A review of available methods and development on energy storage; technology update. *Renew. Sustain. Energy Rev.* **2014**, *33*, 532–545.
4. Vazquez, S.; Lukic, S.M.; Galvan, E.; Franquelo, L.G.; Carrasco, J.M. Energy storage systems for transport and grid applications. *IEEE Trans. Ind. Electron.* **2010**, *57*, 3881–3895.
5. Worku, M.Y.; Abido, M.A.; Iravani, R. Power fluctuation minimization in grid connected photovoltaic using supercapacitor energy storage system. *J. Renew. Sustain. Energy* **2016**, *8*, 013501.
6. Tani, A.; Camara, M.B.; Dakyo, B. Energy Management in the Decentralized Generation Systems Based on Renewable Energy—Ultracapacitors and Battery to Compensate the Wind/Load Power Fluctuations. *IEEE Trans. Ind. Appl.* **2015**, *51*, 1817–1827.
7. Khare, V.; Nema, S.; Baredar, P. Solar–wind hybrid renewable energy system: A review. *Renew. Sustain. Energy Rev.* **2016**, *58*, 23–33.
8. Rodrigues, E.; Godina, R.; Santos, S.F.; Bizuayehu, A.W.; Contreras, J.; Catalão, J. Energy storage systems supporting increased penetration of renewables in islanded systems. *Energy* **2014**, *75*, 265–280.
9. Kim, S.H.; Choi, W.; Lee, K.B.; Choi, S. Advanced dynamic simulation of supercapacitors considering parameter variation and self-discharge. *IEEE Trans. Power Electron.* **2011**, *26*, 3377–3385.
10. Gualous, H.; Louahlia, H.; Gallay, R. Supercapacitor characterization and thermal modelling with reversible and irreversible heat effect. *IEEE Trans. Power Electron.* **2011**, *26*, 3402–3409.
11. Díaz-González, F.; Sumper, A.; Gomis-Bellmunt, O.; Villafáfila-Robles, R. A review of energy storage technologies for wind power applications. *Renew. Sustain. Energy Rev.* **2012**, *16*, 2154–2171.
12. Lambert, S.; Pickert, V.; Holden, J.; Li, W.; He, X. Overview of supercapacitor voltage equalisation circuits for an electric vehicle charging application. In Proceedings of the 2010 IEEE Vehicle Power and Propulsion Conference, Lille, France, 1–3 September 2010; pp. 1–7.
13. Hua, C.C.; Fang, Y.H.; Li, P.H. Charge equalisation for series-connected LiFePO4 battery strings. *IEEE Trans. Power Electron.* **2015**, *8*, 1017–1025.
14. Park, H.S.; Kim, C.H.; Park, K.B.; Moon, G.W.; Lee, J.H. Design of a charge equalizer based on battery modularization. *IEEE Trans. Veh. Technol.* **2009**, *58*, 3216–3223.
15. Kim, J.; Shin, J.; Chun, C.; Cho, B.H. Stable configuration of a Li-ion series battery pack based on a screening process for improved voltage/SOC balancing. *IEEE Trans. Power Electron.* **2012**, *27*, 411–424.
16. Uno, M.; Tanaka, K. Accelerated charge-discharge cycling test and cycle life prediction model for supercapacitors in alternative battery applications. *IEEE Trans. Ind. Electron.* **2012**, *59*, 4704–4712.
17. Lisbona, D.; Snee, T. A review of hazards associated with primary lithium and lithium-ion batteries. *Process Saf. Environ. Prot.* **2011**, *89*, 434–442.
18. Raman, S.R.; Xue, X.D.; Cheng, K. Review of charge equalization schemes for Li-ion battery and super-capacitor energy storage systems. In Proceedings of the 2014 International Conference on Advances in Electronics, Computers and Communications (ICAECC), Bangalore, India, 10–11 October 2014; pp. 1–6.
19. Rahimi-Eichi, H.; Ojha, U.; Baronti, F.; Chow, M. Battery management system: An overview of its application in the smart grid and electric vehicles. *IEEE Ind. Electron. Mag.* **2013**, *7*, 4–16.

20. Thounthong, P.; Chunkag, V.; Sethakul, P.; Sikkabut, S.; Pierfederici, S.; Davat, B. Energy management of fuel cell/solar cell/supercapacitor hybrid power source. *J. Power Sourc.* **2011**, *196*, 313–324.
21. Pegueroles-Queralt, J.; Bianchi, F.D.; Gomis-Bellmunt, O. A Power Smoothing System Based on Supercapacitors for Renewable Distributed Generation. *IEEE Trans. Ind. Electron.* **2015**, *62*, 343–350.
22. Gee, A.M.; Robinson, F.V.P.; Dunn, R.W. Analysis of Battery Lifetime Extension in a Small-Scale Wind-Energy System Using Supercapacitors. *IEEE Trans. Energy Convers.* **2013**, *28*, 24–33.
23. Kollimalla, S.K.; Mishra, M.K.; Narasamma, N.L. Design and Analysis of Novel Control Strategy for Battery and Supercapacitor Storage System. *IEEE Trans. Sustain. Energy* **2014**, *5*, 1137–1144.
24. Thounthong, P.; Luksanasakul, A.; Koseeyaporn, P.; Davat, B. Intelligent Model-Based Control of a Standalone Photovoltaic/Fuel Cell Power Plant With Supercapacitor Energy Storage. *IEEE Trans. Sustain. Energy* **2013**, *4*, 240–249.
25. Beardsall, J.C.; Gould, C.A.; Al-Tai, M. Energy storage systems: A review of the technology and its application in power systems. In Proceedings of the 2015 50th International Universities, Power Engineering Conference (UPEC), Stoke-on-Trent, UK, 1–4 September 2015; pp. 1–6.
26. Kim, C.H.; Kim, M.Y.; Park, H.S.; Moon, G.W. A modularized two-stage charge equalizer with cell selection switches for series-connected lithium-ion battery string in an HEV. *IEEE Trans. Power Electron.* **2012**, *27*, 3764–3774.
27. Ma, T.; Yang, H.; Lu, L. Development of hybrid battery–supercapacitor energy storage for remote area renewable energy systems. *Appl. Energy* **2015**, *153*, 56–62.
28. Phung, T.H.; Crebier, J.C.; Lembeye, Y. Voltage balancing converter network for series-connected battery stack. In Proceedings of the IECON 2012–38th Annual Conference on IEEE Industrial Electronics Society, Montreal, QC, Canada, 25–28 October 2012; pp. 3007–3013.
29. Thanh, H.P.; Collet, A.; Crebier, J.C. An Optimized Topology for Next-to-Next Balancing of Series-Connected Lithium-ion Cells. *IEEE Trans. Power Electron.* **2014**, *29*, 4603–4613.
30. Uno, M.; Kukita, A. Single-Switch Single-Transformer Cell Voltage Equalizer Based on Forward-Flyback Resonant Inverter and Voltage Multiplier for Series-Connected Energy Storage Cells. *IEEE Trans. Veh. Technol.* **2014**, *63*, 4232–4247.
31. Lim, C.S.; Lee, K.J.; Ku, N.J.; Hyun, D.S.; Kim, R.Y. A modularized equalization method based on magnetizing energy for a series-connected lithium-ion battery string. *IEEE Trans. Power Electron.* **2014**, *29*, 1791–1799.